

Thermoelectric Properties, Effective Mass, Chemical Bonding, and Optical Properties of 1,3,6-trimetylo-alloxazine: C₁₃H₁₂N₄O₂

A. H. Reshak^{1,2}, Jan Chyský³, Sikander Azam^{1,*}

¹ Institute of complex systems, FFPW, CENAKVA, University of South Bohemia in CB, Nove Hradý 37333, Czech Republic

² Center of Excellence Geopolymer and Green Technology, School of Material Engineering, University Malaysia Perlis, 01007 Kangar, Perlis, Malaysia

³ Department of Instrumentation and Control Engineering, Faculty of Mechanical Engineering, CTU in Prague, Technická 4, 166 07 Prague 6, Czech Republic

*E-mail: sikander.physicst@gmail.com

Received: 24 August 2013 / Accepted: 16 October 2013 / Published: 15 November 2013

The thermoelectric properties, electronic band structure, density of states, chemical bonding, optical properties, electrons and holes effective mass of 1,3,6-trimetylo-alloxazine are calculated by using the full potential linear augmented plane wave method, based on the density function theory. Result shows that 1,3,6-trimetylo-alloxazine is an indirect band gap semiconductor. The band gap for LDA, GGA, EVGGA and mBJ are 1.919, 1.984, 2.106, 2.335 eV respectively, the valence bands are mostly attributed to N-s/p, H-s, O-p and C-s electronic states, and the conduction bands are attributed to N-s/p and O-p electronic states. The electrical transport properties and types of carriers of 1,3,6-trimetylo-alloxazine are attributed to N-p and O-p electronic states near the Fermi level. From the electronic charge density nature, the covalency can be clearly seen in the bonds C–N and C–H. From the optical behavior we found that the reflectivity of the investigated compound is smaller. Thermoelectric properties of semi conducting 1,3,6-trimetylo-alloxazine were also reported. 1,3,6-trimetylo-alloxazine compound is approximately large band gap semiconductor with a large p-type Seebeck coefficient. The thermoelectric figure of merit is small because of high electrical resistivity and thermal conductivity.

Keywords: Organic compound, semiconductor, optical properties, thermoelectric

1. INTRODUCTION

Alloxazines (benzo[g]pteridine-2,4(1H,3H)-diones) has an interesting applications like photochemical and thermal isomerization of a ruthenium(II)-alloxazine complex [1], and the use of a thin film of lumichrome to manufacture an optical transistor device made-up on a conductive SnO₂

glass [2]. Lumichrome (7,8-dimethylalloxazine = 7,8-dimethylbenzo[g]pteridine-2,4(1H,3H)-dione) has been recognized as the first default metamorphosis-inducing constituents in ascidians [3,4]. On the contrary, riboflavin, a potential parent compound of lumichrome, has been found dormant in induction of larval metamorphosis. This has been verified that *Sinorhizobium meliloti* bacteria churn out lumichrome that enhances root respiration in alfalfa (*Medicago sativa* L) and also causes a redeeming increase in whole-plant net carbon assimilation [5]. The famous swift degradation of riboflavin to lumichrome below several physiological conditions and the occurrence of riboflavin liberate by rhizosphere bacteria recommend that the events established in the *S. meliloti*-alfalfa may be generally important across many plant–microbe interactions [18]. Corbin, study [6] advocate that riboflavin and lumichrome, possess tremendously good safety profiles is able to inactivate a broad range of viruses and bacteria in platelet concentrates, red blood cells and in fresh frozen plasma.

Photochemical studies of alloxazines revealed that isoalloxazinic form can be obtained when under appropriate circumstances, alloxazines that are unsubstituted at the N(1) position can undergo an excited-state double proton transfer (ESDPT) from N(1) to N(10). The compounds having proton donor and acceptor groups' gives rise to excited state reaction, that are able to form the correct hydrogen bonds with alloxazine molecules [7–12]. Due to active centers of alloxazines at N(10), N(5), N(3) and N(1), and at both carbonyl oxygens at C(4) and C(2), ESDPT study required that derivatives with one or more of such active centers should selectively blocked, especially if no structural information is available about the specific interactions between alloxazine and its environment. It is necessary to certify that modification or blocking of an active centre does not create a derivative with entirely new properties rather make it useless in such comparative work. Study of alloxazines becomes more interesting, from the structural point of view, with and without methyl (or some other) substituent at N(1), which could prevent, for example, an excited-state proton transfer reaction, predicted to involve N(1)H and N(10) centers. By making the substitutions may facilitate to study the reactivity of additional reactive centres. i.e., we will state here the usage of 5-deazalumichrome [13] and lumichrome in such relative studies, and putting lumichrome as substituents with methyl in the position N(1) and/or N(3), namely 1-methyllumichrome, 3-methyl-lumichrome and 1,3-dimethyl-lumichrome [11,12,14,15].

The main focus on the earlier studies was using lumichrome and its derivatives; though, it is interesting to explore that whether other alloxazine derivatives can also endure ESDPT reaction. The assessment of novel alloxazines of unlike properties in comparison to lumichrome, and of their derivatives with blocking groups which has been selectively bring in should give more statistics about the environment of ESDPT in general, and of ESDPT in alloxazines in especially. It is suggested that various alloxazine-type molecules with properties more specific than alloxazine or lumichrome are desirable, having, for example, higher fluorescence quantum yields, better solubility in water, or longer fluorescence lifetimes. As an outcome, in a recent study spectral and photophysical properties of several monomethyl substituted alloxazines have been examined [16]. In 2009 M. Bruszyn'ska et. al. [18] used the time-dependent density functional theory (TD-DFT) calculations [17] for the alloxazines and they correlated the electronic structure changes with the substitution patterns.

To the best of our knowledge no comprehensive work neither experimental nor first principles calculations on the thermoelectric, optical properties, electronic band structure, chemical bonding,

electrons and holes effective mass of 1,3,6-trimetylo-alloxazine have appeared in the literature. Except the work of Bruszyn'ska et. al. [18] in which they measure the X-ray diffraction data and perform some measurements in gas phase also they the did some theoretical calculation using B3LYP functional as implemented in the Gaussian 03 package which is non full potential method, usually in B3LYP functional they ignore the van der Waals interactions which leads to inaccurate results.

Table 1. Bond lengths

Atoms	Exp	Opt*	Atoms	Exp	Opt*
N1-C11	1.474(2)	1.4666	C4A-C10A	1.428(2)	1.4316
N1-C2	1.384(1)	1.3901	N5-C5A	1.364(1)	1.3560
N1-C10A	1.387(2)	1.3833	C5A-C6	1.433(2)	1.4308
C11-H11A	0.97(2)	1.0949	C5A-C9A	1.431(2)	1.4407
C11-H11B	0.93(2)	1.0901	C6-C61	1.502(2)	1.4960
C11-H11C	0.98(2)	1.0969	C6-C7	1.374(2)	1.3834
C2-O2	1.218(2)	1.2276	C61-H61A	0.95(2)	1.0969
C2-N3	1.405(2)	1.4089	C61-H61B	0.96(2)	1.0993
N3-C31	1.470(2)	1.4627	C61-H61C	0.97(2)	1.0993
N3-C4	1.395(2)	1.3974	C7-H7	0.98(2)	1.0909
C31-H31A	0.94(3)	1.0908	C7-C8	1.422(2)	1.4163
C31-H31B	0.96(2)	1.0975	C8-H8	1.01(1)	1.0927
C31-H31C	0.97(2)	1.0969	C8-C-9	1.371(2)	1.3790
C4-O4	1.214(2)	1.2285	C9-H9	0.96(2)	1.0901
C4-C4A	1.487(2)	1.4839	C9-C9A	1.419(2)	1.4163
C4A-N5	1.320(2)	1.3215	C9A-N10	1.364(2)	1.3589
N10-C10A	1.320(1)	1.3248			

Thus we thought it would be worthwhile to do the calculations taking in to account the importance of including the van der Waals interactions on the results, therefore we have used all electrons full potential linear augmented plane wave method. We notice that our calculated bonds lengths and angles show good agreement with the experimental data [19] as shown in Table 1 and 2. That is attributed to the fact that the molecule in solid state and because the geometry of the solid state structure is subject to intermolecular forces, such as van der Waals interactions and crystal packing forces. Moreover in the solid states, there exists an intermolecular hydrogen bond interaction corresponding with N(1)–H(1) bond. It is well known that in the crystal lattice there are two intermolecular interactions; potentially weak intermolecular interaction and supramolecular interactions. These supramolecular interactions lead to stabilize the crystal structures. Therefore using full potential method is timely and would bring us important insights in understanding the origin of the band structure and densities of states. Hence it is very important to use a full potential method. Therefore, we have investigated the thermoelectric properties, electronic structure, optical properties, chemical bonding, electrons and holes mass effective of 1,3,6-trimetylo-alloxazine. We also present a detailed study of the thermoelectric properties (TE) of semiconducting 1,3,6-trimetylo-alloxazine, such

as electrical resistivity (ρ), Seebeck coefficient (S), thermal conductivity (κ), calculated power factor (S^2/ρ), and thermoelectric Figure of merit (ZT).

Table 2. Bond Angles

Atoms	Exp(°)	Opt*(°)	Atoms	Exp (°)	Opt*(°)
C11-N1-C2	118.2(1)	118.34	C7- C8-H8	116.6(9)	118.29
C11-N1-C10A	118.7(1)	118.84	C7- C8- C9	121.0(1)	121.12
C2-N1-C10A	123.0(1)	122.73	H8- C8- C9	122.4(9)	120.59
N1-C11-H11A	109(1)	108.93	C8- C9-H9	123(1)	122.50
N1-C11-H11B	107(1)	108.31	C8- C9- C9A	119.7(1)	119.35
N1-C11-H11C	111(1)	110.41	H9- C9- C9A	118(1)	118.14
H11A-C11-H11B	111(1)	110.75	C5A- C9A- C9	119.1(1)	119.43
H11A-C11-H11C	109(1)	108.93	C5A- C9A-N10	121.7(1)	121.12
H11B-C11-H11C	109(1)	109.50	C9- C9A- N10	119.2(1)	119.44
N1- C2-O2	122.2(1)	121.94	C61-C6-C7	122.1(1)	121.98
N1- C2-N3	116.8(1)	116.62	C6- C61- H61A	111(1)	110.41
O2- C2-N3	121.1(1)	121.44	C6- C61- H61B	111(1)	111.19
C2- N3- C31	117.4(1)	117.53	C6- C61- H61C	111(1)	110.86
C2- N3- C4	126.1(1)	126.24	H61A- C61- H61B	109(1)	109.16
C31- N3- C4	116.5(1)	116.20	H61A- C61- H61C	107(1)	108.25
N3- C31- H31A	109(1)	107.60	H61B- C61- H61C	107(1)	106.88
N3- C31- H31B	109(1)	109.58	C6- C7-H7	119.9(9)	119.78
N3- C31- H31C	111(1)	109.60	C6- C7- C8	121.7(1)	121.89
H31A- C31- H31B	112(2)	110.34	H7- C7- C8	118.4(9)	118.33
H31A- C31- H31C	107(2)	110.17	C7- C8-H8	116.6(9)	118.29
H31B- C31-H31C	110(1)	109.53	C6- C61- H61C	111(1)	110.86
N3-C4-O4	121.2(1)	120.96	H61A- C61- H61B	109(1)	109.16
N3- C4- C4A	114.5(1)	114.30	H61A- C61- H61C	107(1)	108.25
O4- C4- C4A	124.3(1)	124.74	H61B- C61- H61C	107(1)	106.88
C4- C4A-N5	118.2(1)	118.51	C6- C7-H7	119.9(9)	119.78
C4- C4A-C10A	119.8(1)	119.83	C6- C7- C8	121.7(1)	121.89
N5- C4A-C10A	122.1(1)	121.65	H7- C7- C8	118.4(9)	118.33
C4A-N5- C5A	117.2(1)	117.65	C8- C9-H9	123(1)	122.50
N5- C5A- C6	119.2(1)	119.14	C8- C9- C9A	119.7(1)	119.35
N5- C5A- C9A	120.3(1)	120.51	H9- C9- C9A	118(1)	118.14
C6- C5A- C9A	120.5(1)	120.35	C5A- C9A- C9	119.1(1)	119.43
C5A-C6-C61	119.8(1)	120.16	C5A- C9A-N10	121.7(1)	121.12
C5A-C6-C7	118.0(1)	117.86	C9- C9A- N10	119.2(1)	119.44
C61-C6-C7	122.1(1)	121.98	C9A- N10-C10A	116.3(1)	116.83
C6- C61- H61A	111(1)	110.41	N1- C10A-C4A	119.7(1)	119.96
C6- C61- H61B	111(1)	111.19	C7- C8- C9	121.0(1)	121.12
H8- C8- C9	122.4(9)	120.59			

*This work Exp.....ref [20]

2. METHODOLOGY

2.1. Theoretical framework

The crystal structure of 1,3,6-trimetylo-alloxazine have been studied theoretically using FPLAPW method. The investigated compound has the triclinic symmetry. We make used of the crystallographic data (CCDC 704366) of 1,3,6-trimetylo-alloxazine ($C_{13}H_{12}N_4O_2$), obtained from Cambridge Crystallographic database [19]. It belongs to the space group P1(# 2) and contains two molecules per unit cell. We have used the lattice parameters $a=8.0460(16)$ Å, $b=8.3362(16)$ Å, $c=9.465(2)$ Å, $\alpha=112.71(2)$, $\beta=96.73(3)$ and $\gamma=100.50(2)$. The crystal structure of 1,3,6-trimetylo-alloxazine has been shown in Fig. 1. Fig. 1 (a) shows the molecular structure of 1,3,6-trimetylo-alloxazine and (b) C–H \cdots O hydrogen bonds.

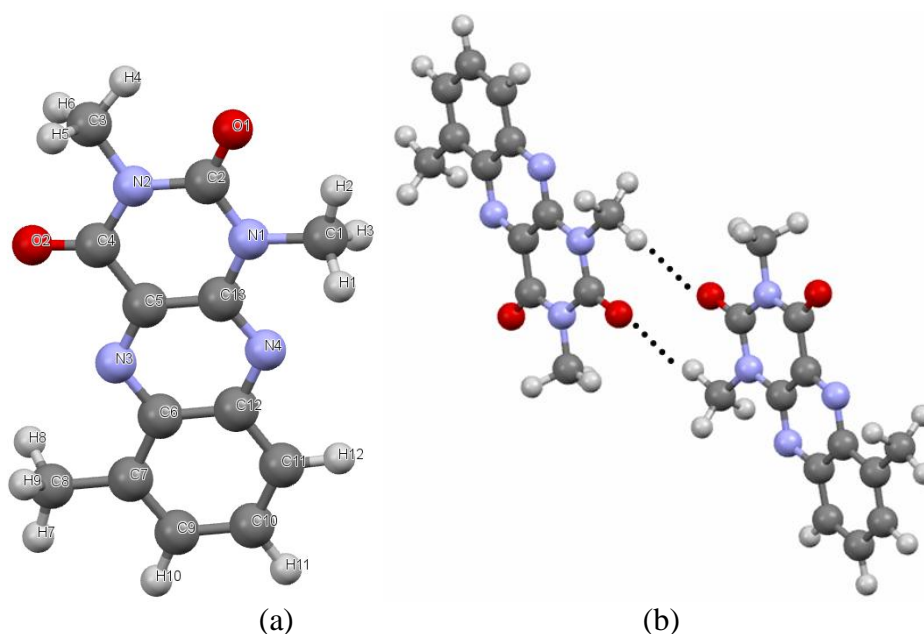


Figure 1. (a) Molecular structure of 1,3,6-trimetylo-alloxazine and (b) C–H \cdots O hydrogen bonds

2.2. Calculation method

The self-consistent calculations were carried out using Wien2k code [20], a full-potential augmented plane wave method. The calculations are based on the local density approximation (LDA), generalized gradient approximation (GGA) of Perdew–Burke–Ernzerh of (PBE), EVGGA as amended by Engel Vosko and modified Becke and Johnson (mBJ) in order to estimate the sensitivity of the results to exchange correlation [21–24]. The sphere radii used were 1.080 a.u. for C and O, 0.580 a.u. for H and 1.180 a.u. for N, respectively. The Brillouin zone integration was carried out by using the modified tetrahedron method [25]. Well converged solutions were obtained with $RMT \times K_{max}=7.0$ (where RMT is the smallest of the muffin-tin radii and K_{max} is the plane wave cut-off) and k-point sampling was checked. One hundred and forty seven k -points in the irreducible wedge of the simple triclinic Brillouin zone were used.

2.3. Theoretical description of optical properties

The optical response functions of solids are frequently described by the complex dielectric function $\varepsilon(\omega) = \varepsilon_1(\omega) + i\varepsilon_2(\omega)$ or by the complex refractive index: $N(\omega) = n(\omega) + ik(\omega)$.

$$\varepsilon_1(\omega) = n^2 - k^2 \dots\dots (1)$$

$$\varepsilon_2(\omega) = 2nk \dots\dots (2)$$

In arguing the interaction between light and solid, one generally uses adiabatic approximation and single-electron approximation. Since the transition frequencies both in-band and between bands are much larger than the phonon frequency in the calculation of electronic structure and the method used is single-electron approximation, the phonon participation in the indirect transition process can be ignored, with only the electronic excitation considered. According to the definitions of direct transition probabilities and Kramers–Kronig dispersion relations, one can deduce the imaginary and the real parts of the dielectric function, absorption coefficient, reflectivity and complex optical conductivity [26–28]. Consider the theoretical formula:

$$\varepsilon_2(\omega) = \frac{\pi e^2}{\varepsilon_0 m^2 \omega^2} \sum_{v,c} \left\{ \int_{\text{BZ}} \frac{2dk}{(2\pi)^2} |a \times M_{v,c}|^2 \delta[E_c(k) - E_v(k) - \hbar\omega] \right\} \dots\dots (3)$$

$$\varepsilon_1(\omega) = 1 + \frac{2e}{\varepsilon_0 m^2} \times \varepsilon_{v,c} \int_{\text{BZ}} \frac{2dk}{(2\pi)^2} \frac{|a \times M_{v,c}(k)|^2}{E_c(k) - E_v(k) / \hbar} \times \frac{1}{[E_c(k) - E_v(k)]^2 / \hbar^2 - \omega^2} \dots (4)$$

$$\alpha(\omega) = \frac{2k\omega}{c} = \frac{2\pi k}{\lambda_0} \dots\dots (5)$$

$$R(\omega) = \frac{(n-1)^2 + k^2}{(n+1)^2 + k^2} \dots\dots (6)$$

Where 'n' is the refractive index, k is the extinction coefficient, ε_0 is the vacuum dielectric constant, λ_0 is the wavelength of light in vacuum, C and V are the conduction band and valence band respectively, BZ is the first Brillouin zone, K is the electron wave vector, 'a' is the unit direction vector of the vector potential A, $M_{v,c}$ is the transition matrix element, ω is the angular frequency, and $E_c(\omega)$ and $E_v(\omega)$ are the intrinsic energy level of the conduction band and valence band respectively.

3. RESULTS AND DISCUSSION

3.1. Band structure

Now we turn our attention to study the electronic properties of 1,3,6-trimetylo-alloxazine compound by calculating the energy band structure and density of states. In Fig. 1, we show the electronic band dispersion curves of the investigated compound along some high symmetry directions of the Brillouin zone calculated within the LDA, GGA, EVGGA and mBJ approximation. In which the dotted line represents the Fermi level. From the band structure, it is cleared that the conduction band minimum is located at U point and the top of the valence band is located at Γ point of the Brillouin zone, showing that 1,3,6-trimetylo-alloxazine is an indirect band gap semiconductor.

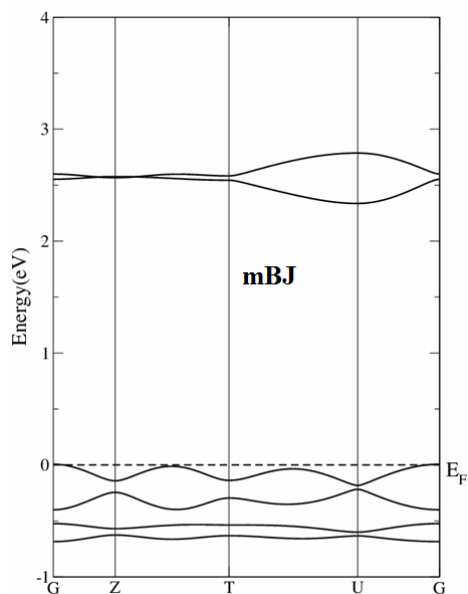
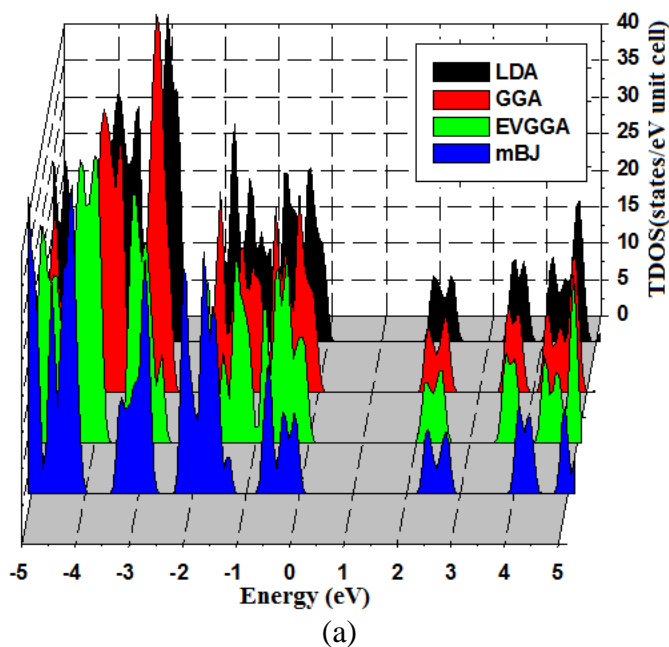


Figure 2. Calculated band structure.

The calculated band gap for LDA, GGA, EVGGA and mBJ are 1.919, 1.984, 2.106, 2.335 eV respectively. It has been recognized that in the self consistent band structure calculation within density functional theory approaches that GGA and LDA usually under estimates the energy gap. That is attributed to the fact that they are simplified model assumptions which are not suitably elastic to exactly reproduce Exc energy. This shortcoming was overcome by the modified Becke–Johnson (mBJ) approach. Which are capable of having better energy gap. The mBJ yields an improved band splitting compared to LDA, GGA and EVGGA [29-34]. Thus, for this motive we will discuss the results obtained by mBJ only.

3.2. Electronic density of states



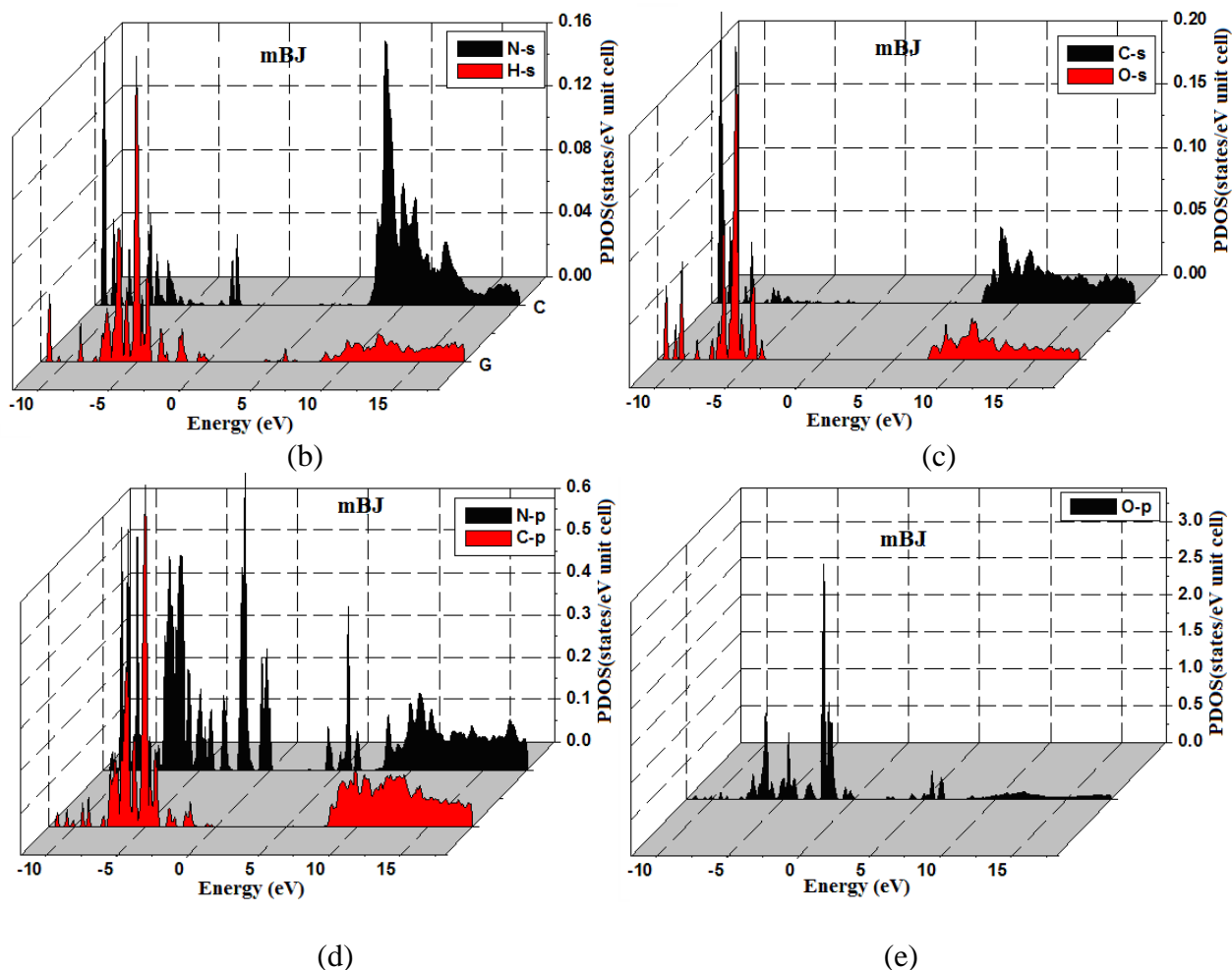


Figure 3. Calculated total and partial densities of states (States/eV unit cell)

In this part we analyze the density of states of the triclinic 1,3,6-trimetylo-alloxazine. The total and partial densities of states (TDOS and PDOS) are shown in Fig. 3. It can be seen that the valence band of 1,3,6-trimetylo-alloxazine is composed of three parts, the lower valence bands from -12.0 eV to -9.0 eV which is composed due to the greater contribution of N-s/p and C-s orbital with smaller contribution of H-s and O-s orbital. The 2nd valence bands part from -8.0 eV to -4.0 eV is composed due to the major contribution of H-s, C-p, O-s/p and N-p orbital with smaller contribution of N-s and C-s orbital electrons. The lower valence bands are mainly attributed due to O-s/p and N-p orbital electrons. Conduction bands are mainly attributed to N-s/p, and O-p orbital electrons and a small number of C-s/p and C-s/p orbital electrons. Therefore, the valence bands are mainly attributed to N-s/p, H-s, O-p and C-s orbital electrons; the conduction bands are mainly attributed to N-s/p, and O-p orbital electrons; and the electrical transport properties of 1,3,6-trimetylo-alloxazine and the types of carrier are mainly attributed to N-p and O-p state electrons. There exists a strong hybridization at -11.0 eV, -9.0 eV and at -2.0 eV between N-s and H-s orbital. Also between -12.0 to -8.0 eV there is a strong hybridization between C-s and O-s orbitals and between N-p and C-p orbitals.

3.3. Electronic charge density

Figs. 4 (a) and (b) shows the calculated total charge density of 1,3,6-trimetylo-alloxazine bonds in (1 1 0) crystallographic plane. We also presented the density difference distributions to analyze bonding in the crystal. A definition of ionic and covalent bonding based on density difference distributions is presented in Figs. 4 (a) and (b). There is a covalent bonding between C–N and C–H. For the other atoms like H and O, H atom shows ionic nature with very weak charge density and the O atom shows no contribution in this plane.

We also calculated the electronic charge density in the (3 2 0) crystallographic plane in order to show the anisotropy in the electronic charge density in the crystal planes. As it is clear from the two plane spectra that the O atom which does not contribute in the (1 1 0) crystallographic plane making covalent bonding with the C atom in (3 2 0) plane. In (3 2 0) plane C–C atom shows covalent bonding which is absent in the (1 1 0). The charge density contour around the H atom in the (1 1 0) plane is completely circular but in the (3 2 0) plane the contour around the H is dumbbell shape but comparatively shows maximum charge density than the (1 1 0) plane. In the crystal structure there are layers of molecules (Fig. 1b) connected by relatively strong hydrogen bonding (C–H····O). A hydrogen bond is the electromagnetic attractive interaction between polar molecules in which hydrogen atom is bound to a highly electronegative atom, such as nitrogen, oxygen or fluorine.

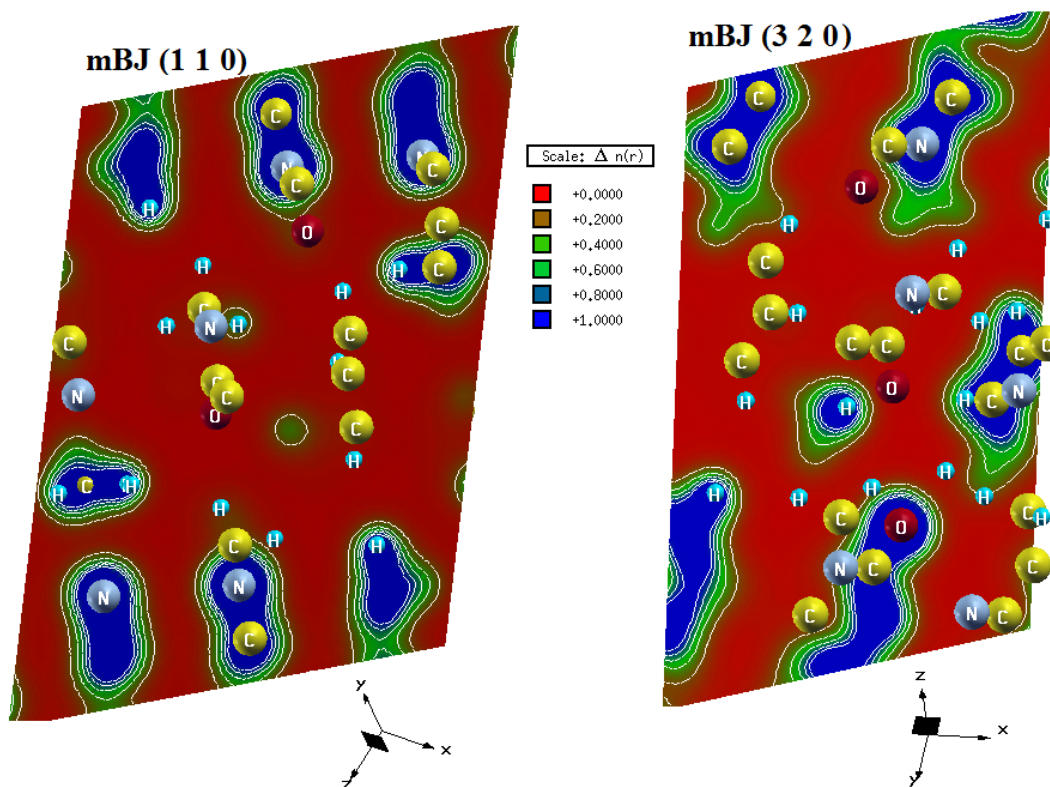


Figure 4. Electronic charge density contour for mBJ.

The hydrogen bond is much stronger than a van der Waals interaction, but weaker than covalent or ionic bonds. This type of bond can occur both in inorganic and organic molecules.

3.4. Effective mass

The electrical transport performance of semi conductor material furthermore can be assessed based on the quasi-classical approach of effective mass approximation, in which the mobility of carriers is taken to be inversely proportional to their effective mass (m^*), such as electron effective mass or hole effective mass. The effective mass obtained from the band structure called effective band mass, was estimated in the one-band-approximation from the curvature band at extreme points in k-space (usually Γ point); or in other words, parts of the band mass, i.e. conduction band minimum (CBM) or valence band maximum (VBM), were fitted by parabolic curves as

$$\frac{1}{m_{B,i,j}} = \frac{2}{\hbar^2} \cdot \frac{d^2 E_{i,j}}{dk_{i,j}^2} \quad \dots\dots\dots (7)$$

with Planck's constant \hbar .

Electron effective mass for 1,3,6-trimetylo-alloxazine is obtained from the curvature of the conduction band at Γ point. We have enlarged the band structures of 1,3,6-trimetylo-alloxazine as illustrated in Figure 2.

The value of calculated electron effective mass ratio $\left(\frac{m^*}{m_e}\right)$ for 1,3,6-trimetylo-alloxazine in $T \rightarrow \Gamma$ direction is 0.09647. We also calculated effective mass ratio of the heavy holes m_{hh}^*/m_e (0.05841) and light holes m_{lh}^*/m_e (0.0268) for the investigated compound in $Z \rightarrow U$ and $\Gamma \rightarrow T$ directions are and.

3.5. Optical properties

3.5.1. Dielectric function

The optical spectroscopy analysis of is a powerful tool to determine of the overall band behavior of a solid [36-38]. Understanding of electronic structures can be reach by investigating the optical spectra which not only give reports about the occupied and unoccupied states, but also about the feature of the bands. Thus we intended to investigate the optical properties of 1,3,6-trimetylo-alloxazine compound. Dielectric function as a connection connecting the microscopic physical transitions between bands to the electronic structures of a solid reflects the band structure of the solid and data about its spectrum. 1,3,6-trimetylo-alloxazine as a semiconductor material, its spectrum generated by electronic transitions between energy levels and all dielectric peaks can be explained by the energy band structure and DOS. Fig. 5a and b, shows the spectrum of the real and imaginary parts of the complex dielectric function versus the photon energy. Our analysis of the $\epsilon_2(\omega)$ curve (Fig. 5a) shows that the first critical point of the dielectric function occurs at 1.90 eV.

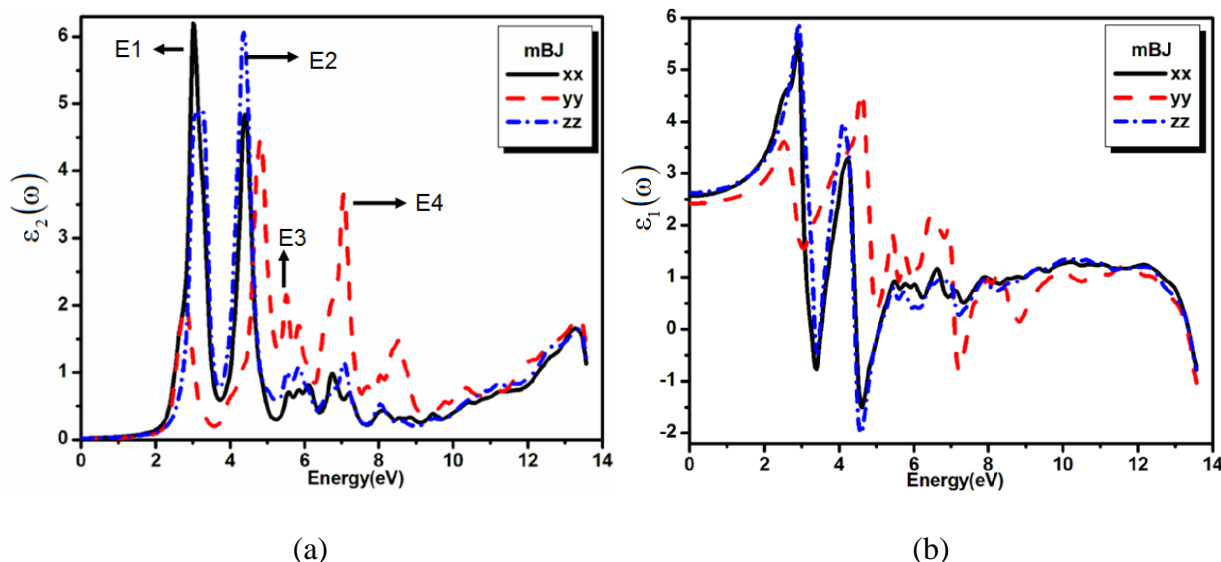


Figure 5. Calculated imaginary $\varepsilon_2(\omega)$ and real part $\varepsilon_1(\omega)$ of dielectric tensor

This point is Γ v–Uc, which gives the threshold for the optical transitions between the VBM and the CBM. This is known as the fundamental absorption edge. Beyond this threshold energy (first critical point), the curve increases rapidly. This is due to the fact that the number of points contributing towards $\varepsilon_2(\omega)$ is increased abruptly. The main peak of $\varepsilon_2^{xx}(\omega)$, $\varepsilon_2^{yy}(\omega)$ and $\varepsilon_2^{zz}(\omega)$ spectrum is situated at about 2.8 eV.

Table 3. Static dielectric constants

$n(0)$	$\varepsilon_1(0)$	$\hbar\omega_p$
$n^{xx}(0)=1.602$	$\varepsilon^{xx}(0)=2.566$	$\hbar\omega_p^{xx} = 3.515$
$n^{yy}(0)=1.555$	$\varepsilon^{yy}(0)=2.418$	$\hbar\omega_p^{yy} = 7.463$
$n^{zz}(0)=1.619$	$\varepsilon^{zz}(0)=2.623$	$\hbar\omega_p^{zz} = 3.482$

The observed structure at Fig. 5a, show there exists second pronounced peak and two small peaks, these peaks have been marked as E1, E2, E3, and E4. Following Fig. 5b, it can be seen that at the low-energy region the real part of the dielectric constant increases with energy, and reach its first peak for $\varepsilon_1^{xx}(\omega)$ at 2.486 eV, $\varepsilon_1^{yy}(\omega)$ at 2.221 eV and $\varepsilon_1^{zz}(\omega)$ at 2.498 eV. By the Kramers–Kronig relationship, $\varepsilon_1(\omega)$ can be attained by integration over a fairly wide frequency range using a differential coefficient of $\varepsilon_2(\omega)$. Therefore, $\varepsilon_1(\omega)$ reaches its peak at the maximum slope of $\varepsilon_2(\omega)$, rises and drops respectively and intersects the real axis. The height of the peaks decreasing with the increase of photon energy. The calculated static dielectric constants for $\varepsilon_1^{xx}(0)$, $\varepsilon_1^{yy}(0)$ and $\varepsilon_1^{zz}(0)$ are given in Table 3.

The energy loss function, which describes the loss of energy when electrons pass through a uniform dielectric, can be calculated from the dielectric constant as:

$$L(\omega) = \text{Im} \left(\frac{-1}{\epsilon(\omega)} \right) = \frac{\epsilon_2(\omega)}{[\epsilon_1^2(\omega) - \epsilon_2^2(\omega)]} \dots\dots\dots(8)$$

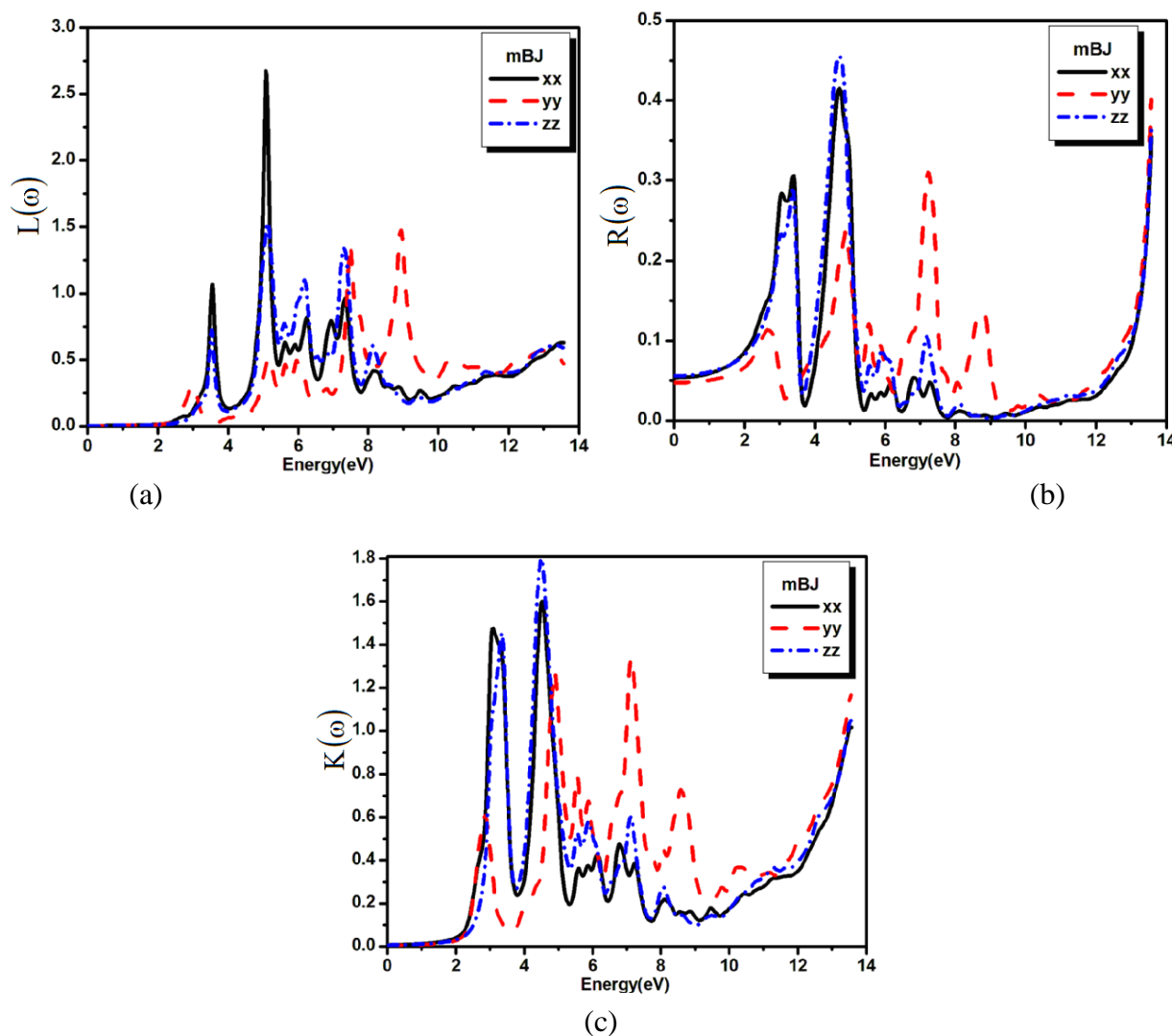


Figure 6. Calculated energy-loss spectrum $L(\omega)$, reflectivity $R(\omega)$ and extinction coefficient $K(\omega)$.

The peak of the loss function represents the characteristic associated with plasma oscillation; the corresponding oscillation frequency is called plasma frequency. Fig. 6a shows the 1,3,6-trimetylo-alloxazine electron energy loss function; it can be seen that the largest energy loss peak occurs at about 5.3 eV, which corresponds to the edge energy of 1,3,6-trimetylo-alloxazine plasma. Fig. 6b, showing the reflective spectrum of 1,3,6-trimetylo-alloxazine, it is found that the transition between bands occurs mainly in the energy range of 2.0–4.0 eV. The average refractive index is up to 45%, showing that 1,3,6-trimetylo-alloxazine has metal reflective properties in this energy range. Most of the incident

light is reflected when the refractive index is small. This indicates that the N-2s and C-2s state electrons have a very deep level, in agreement with the band structure and the calculated DOS.

A relationship between calculated extinction coefficient $K(\omega)$ and energy is shown in Fig. 7b. The response of $K(\omega)$ for the studied material is closely matched to the response of $\epsilon_2(\omega)$. A small variation of $K(\omega)$ from $\epsilon_2(\omega)$ is due to the fact that this generalization is not valid for the medium with some absorption coefficient [35].

3.5.2. Birefringence

The refractive index and the extinction coefficient spectra are shown in Fig. 7a and b. The main peaks of $n(\omega)$ are in the energy range between 2.0 and 4.0 eV. The refractive index decreases with the increase of photon energy. We have calculated the refractive index at the static limit along the x, y, and z crystallographic axes and the obtained values are given in Table 3. The refractive indices (Fig.7a) of the crystal is closely related to the electronic polarizability of ions and the local field inside the crystal. The average value of $n(0)$ is equal to 1.592. Looking at Fig. 6a, a maximum can be observed in the spectrum between 3.0 and 5.5 eV. At intermediate energies many small peaks appear and then the curves vanish at higher energies. The reason for these vanishing curves at higher energy is due to the fact that beyond certain energy the material can no longer act as transparent material and it absorbs high energy photons. It is also clear from Fig. 7a that the refractive index falls below unity at number of frequencies.

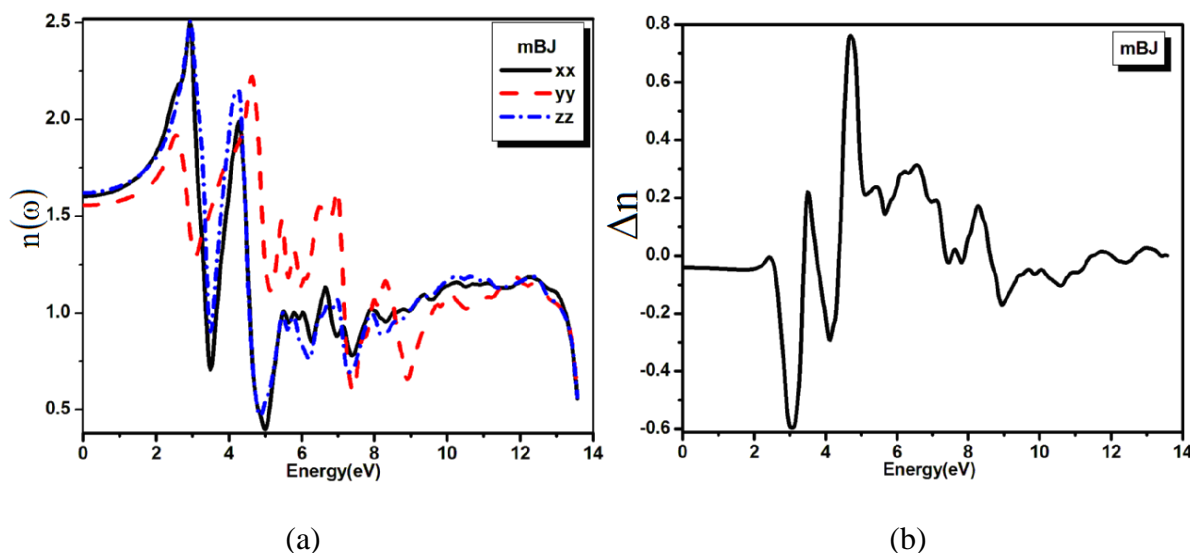


Figure 7. Calculated refractive index $n(\omega)$ and birefringence.

Refractive index lesser than unity shows that the phase velocity of light is greater than the light celerity C , which might seem to imply a contradiction to relativity. However, this overlooks the fact that a signal must be transmitted as a wave packet rather than a monochromatic wave. The linear

optical susceptibilities of 1,3,6-trimetylo-alloxazine compounds displays substantial anisotropy, which turns (favors) an important amount of second harmonic generation (SHG) and optical parametric oscillator (OPO) effectiveness due to better fulfilling of phase equivalent situation, resolute by birefringence [35]. The birefringence is the distinction between the extraordinary and ordinary refraction indices, $\Delta n = n_e - n_o$, where n_e and n_o are the indices of refraction for an electric field oriented along and perpendicular to the *c*-axis. The refractive index is assessed by the expression [36].

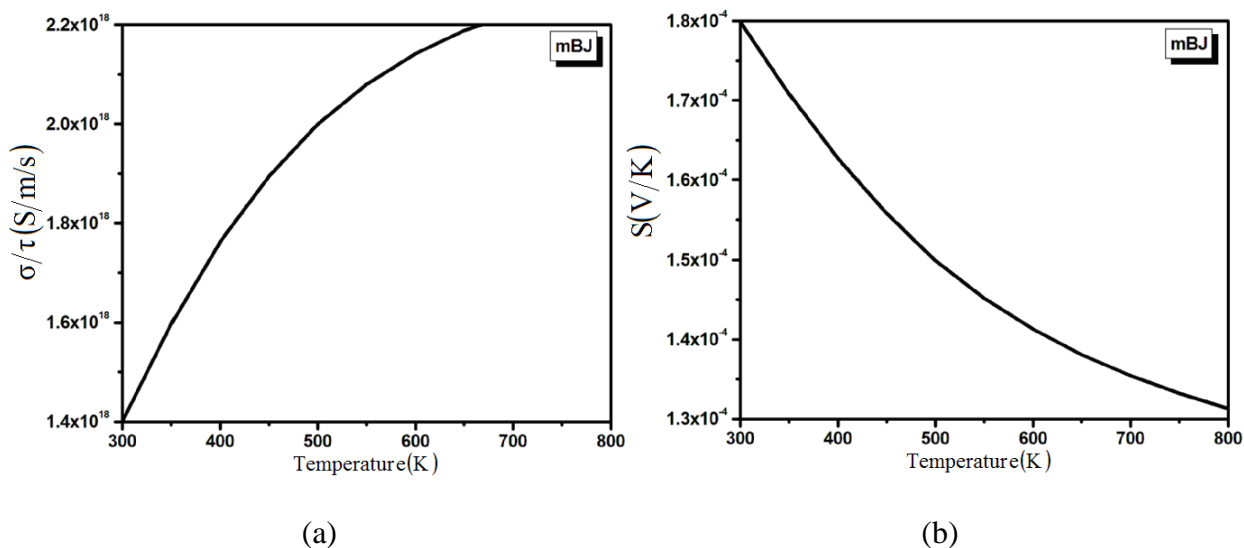
Fig. 7b shows the dispersal of the birefringence $\Delta n(\omega)$ for the 1,3,6-trimetylo-alloxazine compound. It is motivating in the nonabsorbing region, at energies below the energy gap. The $\Delta n(\omega)$ spectral dependence shows strong oscillations around zero in the energy range up to 13.7 eV. We have found that the static limit of birefringence $\Delta n(0)$ is equal to -0.045.

4. THERMOELECTRIC PROPERTIES

In past few years much work has been done to identify high performance thermoelectric materials for applications in power generation and device cooling. The efficiency of a thermoelectric device generally improves by increasing the material's thermoelectric figure of merit $ZT = \frac{S^2 \sigma}{\kappa} T$, where T is the temperature, σ is the electrical conductivity, S the Seebeck coefficient (thermopower) and κ is the thermal conductivity. For metals or degenerate semiconductors the Seebeck coefficient is proportional to temperature, effective mass m^* and inversely proportional to the charge carrier concentration n . In the approximation of energy independent scattering, the relationship is given by

$$S = \frac{8\pi k_B^2}{3eh^2} m^* T \left(\frac{\pi}{3n} \right)^{3/2}$$

Where K_B Boltzmann's constant, e is the charge of an electron and h is Planck's constant.



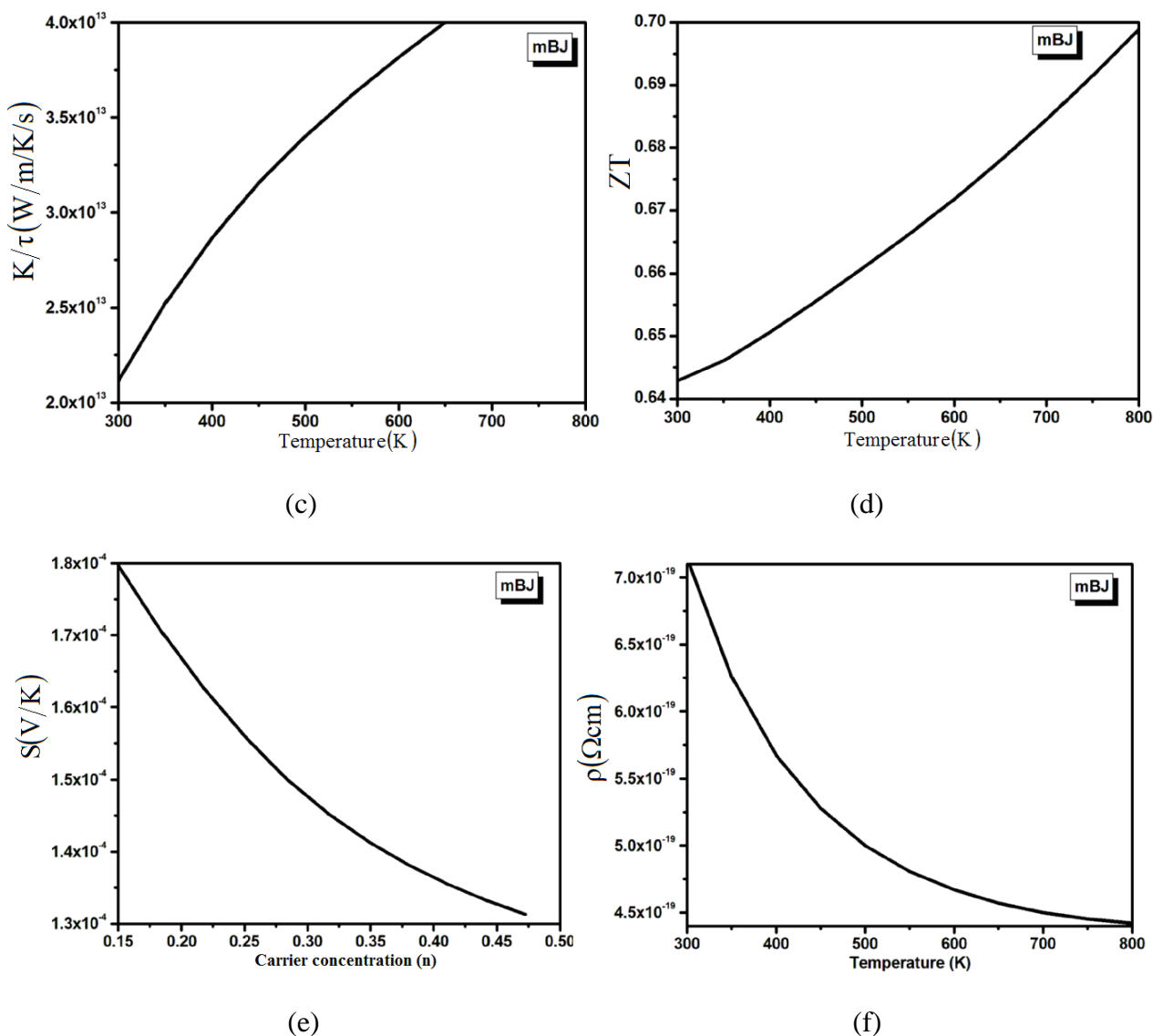


Figure 8. Calculated thermoelectric properties; Seebeck coefficients, electrical conductivity, thermal conductivity and figure of merit.

Thus, large seebeck coefficient S translates to large effective mass which is equivalent to large density-of-states or flat bands at the Fermi level. Low electrical resistivity (or high electrical conductivity σ) requires a large mobility, μ , and large carrier (electrons or holes) concentration n through

$$1/\rho = \sigma = ne\mu$$

The calculated electrical conductivity versus temperature has been shown in Fig. 8a. The calculated spectra show that with the increase in temperature the conductivity of the material also increased and reaches to its maximum at 675 K temperature. The increase in the electrical conductivity means that there are greater concentrations of carriers which will cause a decrease in seebeck coefficient. That corresponds that the electrical conductivity is greater at higher temperatures, which shows that the electron is thermally excited to the conduction bands. The calculated seebeck coefficient S of 1,3,6-trimetylo-alloxazine as a function of temperature is shown in Fig. 8b. This has a

large p-type Seebeck coefficient. The magnitude of the seebeck coefficient (S) temperature dependent below 400 K, and rapidly decreasing toward zero above 400 K. this gradual decrease of the Seebeck coefficient is due to the thermal excitation of electrons across the band gap. Holes are being the majority carriers are consistent with their higher mobility and smaller effective mass than the electron carriers. However, it is visible from the Fig. 8b that the S falls rapidly than σ , which illustrates the bipolar effect which take place when many bands contribute to carrier transport and is mostly strong in electron and hole band. This conduction (hole) radically reduces the seebeck coefficient because the holes carry the opposite charge from electrons. This effect will also increased the thermal conductivity spectra which has been also calculated for 1,3,6-trimetylo-alloxazine as plotted in Fig. (8c). The thermal conductivity increases with increasing temperature this is mainly brought on by an increase in the electronic contribution. In Fig. 8d, we present the dimensionless figure of merit (ZT) for 1,3,6-trimetylo-alloxazine from 300 K to 800 K. The potential of a material for thermoelectric applications is determined in large part to a measure of the material's dimensionless figure of merit. High mobility carriers are most enviable in order to have the highest electrical conductivity. Semiconductors have been primarily the materials of choice for thermoelectric applications. The best thermoelectric materials that are currently used in the devices have a value of $ZT \approx 1$. The value ZT_{\max} for 1,3,6-trimetylo-alloxazine was 0.70 at 800 K. So from the ZT spectra it is cleared that our investigated compound can not be used in thermoelectric applications. The variation of the Seebeck coefficient with the carrier concentration (n) is shown in Fig. 8(e). The variation of S with n is found to fit a model assuming transport by single parabolic band (SPB) with acoustic phonon scattering and a band effective mass (m^*) of 0.8778 m_e . The seebeck coefficient has greater value at low concentrations but as the carrier concentration are increased the seebeck coefficient decreases. Figure 8g shows the temperature dependent electrical resistivity of 1,3,6-trimetylo-alloxazine. Transport behavior changes in the whole selected range temperature. The resistivity drops rapidly with increasing temperature below 300 K indicating a semiconducting behavior.

5. CONCLUSION

We have carried out a systematic ab initio study of the electronic structure, band structures, density of states, and the linear optical properties of 1,3,6-trimetylo-alloxazine compound by using the first-principles FP-LAPW method within LDA, GGA, EVGGA and mBJ approximations. Our results for the band structure and DOS show that this compound is a semiconductor with an indirect band gap, the band gap for LDA, GGA, EVGGA and mBJ are 1.919, 1.984 2.106 and 2.335 eV respectively. From the electronic charge density the covalency can be clearly seen in the bonds between C–N and C–H and the H atom shows the ionic nature. The effective mass ratio for electron, heavy hole and light hole also calculated in $T \rightarrow \Gamma$, $Z \rightarrow U$ and $\Gamma \rightarrow T$ direction are 0.09647, 0.05841 and 0.0268. The imaginary and real parts of the frequency dependent dielectric function and the reflectivity show a considerable anisotropy. Also, the results for the dielectric static constant and refractive index in the limit of zero frequency are calculated.

We also presented transport properties of 1,3,6-trimetylo-alloxazine compound by first-principles electronic structure calculations in conjunction with the semi-classical Boltzmann theory, and the results are discussed. The value ZT_{\max} for 1,3,6-trimetylo-alloxazine was 0.70 at 800 K, which is clear that our investigated compound is not good for thermoelectric properties. Based on the calculated Seebeck coefficient, electrical and thermal conductivity and power factor of 1,3,6-trimetylo-alloxazine compound as a function of Temperature, the maximum power factors and the ZT are estimated, and it can offer useful guidelines that by doping the thermoelectric properties can be improved of this compound.

ACKNOWLEDGMENT

This work was supported from the project CENAKVA (No. CZ.1.05/2.1.00/01.0024), the grant No. 143/2013/Z of the Grant Agency of the University of South Bohemia. School of Material Engineering, Malaysia University of Perlis, P.O Box 77, d/a Pejabat Pos Besar, 01007 Kangar, Perlis, Malaysia.

References

1. S. Miyazaki, T. Kojima, S. Fukuzumi, *J. Am. Chem. Soc.* 130 (2008) 1556.
2. Y.H. Zen, C.M. Wang, *J. Chem. Soc., Chem. Commun.* (1994) 2625.
3. S. Tsukamoto, H. Kato, H. Hirota, N. Fusetani, *Biol. Ascidians* (2001) 335.
4. S. Tsukamoto, H. Kato, H. Hirota, N. Fusetani, *Eur. J. Biochem.* 264 (1999) 785.
5. D.A. Phillips, C.M. Joseph, G.P. Yang, E. Martinez-Romero, J.R. Sanborn, H. Volpin, *Proc. Natl. Acad. Sci. USA* 96 (1999) 12275.
6. F. Corbin, *Int. J. Hematol.* 76 (2002) 253.
7. E. Sikorska, A. Koziolowa, *J. Photochem. Photobiol. A* 95 (1996) 215.
8. M. Kasha, *J. Chem. Soc., Faraday Trans. II* 82 (1986) 2379.
9. P.S. Song, M. Sun, A. Koziolowa, J. Koziol, *J. Am. Chem. Soc.* 96 (1974) 4319.
10. A. Koziolowa, *Photochem. Photobiol.* 29 (1979) 459.
11. E. Sikorska, I.V. Khmelinskii, M. Kubicki, W. Prukala, M. Hoffmann, I.F. Machado, L.F.V. Ferreira, J. Karolczak, D.R. Worrall, A. Krawczyk, M. Insinska-Rak, M. Sikorski, *J. Phys. Chem. A* 110 (2006) 4638.
12. E. Sikorska, I.V. Khmelinskii, M. Hoffmann, I.F. Machado, L.F.V. Ferreira, K. Dobek, J. Karolczak, A. Krawczyk, M. Insinska-Rak, M. Sikorski, *J. Phys. Chem. A* 109 (2005) 11707.
13. A. Koziolowa, N.V. Visser, J. Koziol, M.M. Szafran, *J. Photochem. Photobiol. A* 93 (1996) 157.
14. E. Sikorska, I.V. Khmelinskii, W. Prukala, S.L. Williams, M. Patel, D.R. Worrall, J.L. Bourdelande, J. Koput, M. Sikorski, *J. Phys. Chem. A* 108 (2004) 1501.
15. E. Sikorska, J.L. Bourdelande, D.R. Worrall, M. Sikorski, *Pol. J. Chem.* 77 (2003) 65.
16. E. Sikorska, I.V. Khmelinskii, J.L. Bourdelande, A. Bednarek, S.L. Williams, M. Patel, D.R. Worrall, J. Koput, M. Sikorski, *Chem. Phys.* 301 (2004) 95.
17. E. Gross, J. Dobson, M. Petersilka, *Top. Curr. Chem.* 181 (1996) 81.
18. M. Bruszyn'ska et al. / *Chemical Physics* 361 (2009) 83–93
19. Cambridge Crystallographic Data Centre, CCDC, with the deposition No. CCDC-704366. Copies of this information may be obtained free of charge from the Director, CCDC, 12 Union Road, Cambridge CB2 1EZ, UK (fax: +44 1223 336 033; email: deposit@ccdc.cam.ac.uk or <http://www.ccdc.cam.ac.uk>).

20. P. Blaha, K. Schwarz, J. Luitz WIEN97, A full potential linearized augmented plane wave package for calculating crystal properties, Karlheinz Schwarz. Techn. Universit at Wien, Austria, 1991. ISBN:3-9501031-0-4.
21. J. P. Perdew, A. Zunger, *Phys. Rev. B.* 23 (1981) 5048.
22. J. P. Perdew, K. Burke, M. Ernzerhof, *Phys. Rev. Lett.* 77 (1996) 3865.
23. E. Engel, S. H. Vosko. *Phys. Rev. B.* 50 (1994) 10498.
24. F. Tran, P. Blaha. *Rev. Lett.* 102, 226401 (2009).
25. J. A. Wilson and A. D. Yoffe, *Adv. Phys.* 18, 193 (1969).
26. R.C. Fang, Spectroscopy of Solid, University of Science and Technology Press, Hefei, China, 2001, pp. 71–75.
27. X.J. Sheng, *Science Press*, Beijing, 2002, pp. 76–94.
28. Q. Chen, Q. Xie, W.J. Yan, *Sci. China (Ser. G)* 38 (7) (2008) 825–833.
29. A. H. Reshak, H. Kamarudin, I. V. Kityk, S.Auluck. *journal of material science*, 48 (2013) 5157-5162
30. A. H. Reshak, O. Y. Khyzhun, I. V. Kityk, A. O. Fedorchuk, H. Kamarudin, S.Auluck, O.V. Parasyuk. *Sci.Adv. Mater.* 5 (2013) 1-12.
31. Sikander Azam, A. H. Reshak. *Int. J. Electrochem. Sci.*, 8 (2013) 10359 – 10375.
32. A.H. Reshak, S.A. Khan. *Computational Materials Science* 78 (2013) 91–97.
33. Saleem Ayaz Khan, A. H. Reshak. *Int. J. Electrochem. Sci.*, 8 (2013) 9459 – 9473.
34. Ali H. Reshak, S. Auluck, I.V. Kityk. *Current Opinion in Solid State and Materials Science* 12 (2008) 14–18.
35. Wooten F. Optical properties of solids. New York: Academic; (1972).
36. B. Amin, R. Khenata, A. Bouhemadou, I. Ahmad, M. Maqbool. *Physica B.* 407, (2012) 2588–2592
37. B. Amin, I. Ahmad, M. Maqbool, S. Goumri-Said, R. Ahmad. *J. Appl Phys.* 109 (2011) 023109
38. M. Maqbool, B. Amin, I. Ahmad. *J. Opt. Soc. Am. B.* 26(11) (2009) 2181-2184